

# MetaLoc: Learning to Learn Wireless Localization

Jun Gao\*, Dongze Wu\*, Feng Yin\*, Qinglei Kong<sup>†</sup>, Lexi Xu<sup>‡</sup>, Shuguang Cui\*

\*School of Science and Engineering, The Chinese University of Hong Kong, Shenzhen, China

<sup>†</sup>Institute of Space Science and Applied Technology, Harbin Institute of Technology, Shenzhen, China

<sup>‡</sup>Research Institute, China United Network Communications Corporation, Beijing, China

**Abstract**—The existing indoor fingerprinting localization methods are rather accurate after intensive offline calibration for a specific environment, no matter based on received signal strength (RSS) or channel state information (CSI), but the well-calibrated localization model (can be a pure statistical one or a data-driven one) will present poor generalization ability in the highly variable environments, which results in big loss in knowledge and human effort. To break the environment-specific localization bottleneck, we propose a new-fashioned data-driven fingerprinting method for localization based on model-agnostic meta-learning (MAML), named by MetaLoc. Specifically, MetaLoc is characterized by rapidly adapting itself to a new, possibly unseen environment with very little calibration. The underlying localization model is taken to be a deep neural network, and we train an optimal set of environment-specific meta-parameters by leveraging previous data collected from diverse well-calibrated indoor environments and the maximum mean discrepancy criterion. We further modify the loss function of vanilla MAML and propose a novel framework named as MAML-DG, which is able to achieve faster convergence and better adaptation abilities by forcing the loss on different training domains to decrease in similar directions. Experiments from simulation and site survey confirm that the meta-parameters obtained for MetaLoc achieves very rapid adaptation to new environments, competitive localization accuracy, and high resistance to significantly reduced reference points (RPs), saving a lot of calibration effort.

**Index Terms**—Fingerprinting localization, meta-learning, channel state information (CSI), received signal strength (RSS).

## I. INTRODUCTION

Location-based services are ubiquitous and indispensable in our daily lives, and localization techniques have been studied broadly by different research societies for well over a century [2]–[5]. While the existing Global Navigation Satellite Systems (GNSS) have been providing mobile users with high outdoor localization accuracy, emerging applications in all sectors, such as autonomous driving [6], cooperative 3D scene reconstruction [7], and epidemic tracking [8], have demanded increasingly higher requirements for the overall performance of the localization systems, including localization accuracy, environmental adaptability, and robustness. On the other hand, efficient use of mmWave and massive MIMO in 5G/6G also calls for accurate location information for high-throughput transmissions [9]–[11]. It is high time to turn our focus to new-fashioned localization system that can cover outdoor environments and more complex indoor scenes, to achieve a full spectrum of high-precision localization services [12], [13].

Fingerprinting localization method has gradually become a research hotspot in indoor environments, which consists of two stages, i.e., offline stage and online stage. In the offline stage, a fingerprint database is established using measured signal features from multiple access points (APs) that vary with locations, also known as reference points (RPs). Representative features include received signal strength (RSS), channel state information (CSI), and the environmental magnetic field. In the online stage, features measured at an unknown location, also known as test point (TP) are computed with the established database using some algorithms, such as RADAR [14] and Horus [3].

However, wireless signal propagation is sensitive to the minor environment variations, such as opening the door or people walking around, which can result in the recorded fingerprints inconsistency even if the user stays at the same location. Therefore it remains difficult to build an accurate statistical fingerprint database to represent the entire environment of interest. Instead, machine learning can help extract features from system behaviors, making it very promising to develop data-driven localization mechanisms, which has attracted extensive attention from academia and industry in recent years [15]–[17]. Since most of the machine learning techniques are data-hungry and require abundant data samples, it is inevitable to consume a significant amount of time and labor to build a database for each indoor localization environment. To solve this challenge, several well-established machine learning techniques have been utilized in indoor localization, such as data augmentation [18], semi-supervised learning technique [19], informed machine learning [20].

Whereas we have witnessed that most studies of indoor localization to date mainly focus on one individual environment, such as one or a few rooms [14], one building floor [21], or during a specific period [22], little attention has been paid to connections among multiple environments. There is no guarantee that a preselected machine learning model that performs well in one environment can adapt to others elsewhere. When facing a new environment, for example, opening the windows, or people entering a new room, researchers have to reconstruct a new fingerprint database and retrain the machine learning model with the vast amount of measurements collected from the heavy site surveys. Therefore, we expect one machine learning model could learn the essential channel features that are broadly applicable to all indoor environments, as demanded in a recent 6G white paper [13].

This paper is an extension of work [1] originally presented in the proceedings of the IEEE International Conference on Communications (ICC), Seoul, Korea, May 2022.

TABLE I: Comparisons of different localization methods

Methods	Signal Features	Models	Accuracy	Robustness	Cost-effectiveness
FILA [23]	CSI	Deterministic	0.45 m ~ 1.2 m	×	×
DeepFi [24]	CSI	Probabilistic	0.95 m~1.80 m	×	✓
CiFi [25]	CSI	Machine learning	1.50 m~3.00 m	×	✓
ConFi [26]	CSI	Machine learning	1.36 m	×	×
CRISLoc [27]	CSI	Machine learning	0.29 m	✓	×
TransLoc [28]	RSS	Machine learning	1.82 m~2.81 m	✓	×
ViVi [29]	RSS	Deterministic	3.30 m~4.30 m	✓	×
AcMu [30]	RSS	Deterministic	1.40 m~3.00 m	✓	×
Fidora [31]	CSI	Machine Learning	submeter-level	✓	×
DAFI [32]	CSI	Machine Learning	97.6% / 89.3%	✓	×
DFPS [33]	RSS	Machine Learning	1.2m~2.8m	✓	×
ILCL [34]	CSI	Probabilistic	1.28m~2.38m	✓	✓

### A. Related Works

Indoor localization technologies have been developed for many years, and the existing works can be summarized from the views of deterministic, probabilistic, and machine learning localization. The details are as follows.

1) *Probabilistic Localization*: The probabilistic technique utilizes statistical characteristics between the signal measurements and the fingerprint database for localization based on the maximum likelihood. Horus [3] is the most classical probabilistic localization method, by estimating a probabilistic model to express the signal distribution and then obtain the maximum posterior probability of the target location. Furthermore, Yin et al. present a distributed recursive Gaussian process regression framework for constructing RSS map for target tracking with reduced complexity and storage [16]. As highlighted in [17], Bayesian networks for solving RSS-based cooperative localization problem is proposed to infer the marginal posterior of the position. DeepFi [24] incorporates the probabilistic model with the greedy learning algorithm to further reduce computational complexity. In summary, probabilistic localization methods generally have low complexity but rely on precise signal values, which is difficult to guarantee high localization performance in the dynamic environment.

2) *Deterministic Localization*: To estimate the physical position of the target point, deterministic methods mainly utilize the similarity metric in the signal space, and the target point is located as its closest fingerprint location in the space. Traditional deterministic method is implemented based on k nearest neighbors (KNN), in which various similarity measures can be leveraged to assess the fingerprint similarity, such as Euclidean distance [29] and its temporal weighted version, cosine similarity [35], and Tanimato similarity [36]. Some other more advanced deterministic algorithms such as support vector machine [37] and linear discriminant analysis [38] can demonstrate better localization accuracy but with higher computational cost. In summary, deterministic localization technologies are easy to implement. However, due to statistical fluctuation of wireless signals, adopting the similarity measures in the online stage may result in a dispersed set of neighbors which are quite distant apart in the physical space.

3) *Machine learning Localization*: Recently, advanced machine learning technologies have emerged in the localization. Hsieh et al. treat the localization as a classification problem using RSS, and various types of neural networks are adopted

to estimate the location of an object in a room [15]. FILA [23] is the first work to extract CSI feature to improve indoor localization performance. Furthermore, ConFi [26] introduces CNN (convolutional neural network), which is most commonly applied to analyze visual imagery, to participate in the localization procedures. It opens up new ideas to explore indoor localization although environmental dynamics challenge the robustness of the approach.

To improve the robustness of the localization, the existing solutions mainly focus on the sides of model and data. For the model-oriented side, domain adaptation methods have been widely utilized, where in general the original environments is the source domain and the changed environment is the target domain. For example, to capture the connections between different domains, TransLoc [28] finds appropriate cross-domain mappings between the common knowledge and domain specific knowledge such that a homogeneous feature space containing discriminative information of different domains can be constructed. CRISLoc [27] employs transfer learning to reconstruct the high-dimensional CSI fingerprint database on the basis of the outdated fingerprints and a few fresh measurements. Fidora [31] first adopts a data augmentor that introduces data diversity using a variational autoencoder. It then trains a domain-adaptive classifier that adjusts itself to newly collected unlabeled data using a joint classification reconstruction structure. ILCL [34] combines broad learning system together with the probabilistic models to achieve environmental adaptation and reduce the training time. Nevertheless, the model tends to be overfitting when the number of CSI images is small. For the data-oriented side, ViVi [29] exploits the spatial gradient among multiple locations to reduce the uncertainty in RSS fingerprints. CiFi [25] uses phase difference between pairs of antennas instead of the raw measurements to improve the stability of the designed CSI fingerprints. Meanwhile, DFPS [33] proposes to combine the raw RSS and RSS difference between pairs of APs to enhance the robustness of localization against the problem of heterogeneous hardware.

Besides, to reduce the cumbersome site surveys in indoor localization, data augmentation has been utilized in [18] to mimic the extensive site surveys, and it creates a fingerprint database with finer granularity but less effort. Besides, applying the emerging semi-supervised learning technique [19] through combining a small number of labeled data with many

TABLE II: Notations

Notation	Description
$\mathcal{P}(\tau)$	Overall distribution of tasks
$\mathcal{P}_i(\tau)$	Distribution of tasks from domain $i$
$f_{\theta}$	Model output with parameter $\theta$
$N$	The number of classes in a task $\tau_i$
$K_{spt}$	The number of samples of the support set under each position in each task
$K_{qry}$	The number of samples of the query set under each position in each task
$D_{\tau_i}^s$	Support set of localization task $\tau_i$ that contains $K_{spt}$ number of samples under each position of $N$ ways
$D_{\tau_i}^q$	Query set of localization task $\tau_i$ that contains $K_{qry}$ number of samples under each position of $N$ ways
$\mathcal{L}_{\tau_i}(f_{\theta}, D_{\tau_i}^s)$	Task-specific loss function for task $\tau_i$ based on model parameter $\theta$ and support set $D_{\tau_i}^s$
$\mathcal{L}_{\tau_i}(f_{\theta}, D_{\tau_i}^q)$	Task-specific loss function for task $\tau_i$ based on model parameter $\theta$ and query set $D_{\tau_i}^q$
$\theta'_i$	Task-specific parameters after the inner loop via one step of gradient descent
$\theta^*$	Updated meta-parameters after the outer loop
$\theta_T(Q)$	Task-specific adapted model parameters obtained by updating $\theta^*$ via $Q$ steps of gradient descent
$\alpha$	Inner learning rate
$\beta$	Outer learning rate
$w$	Weight of the loss function of the second training domain

inexpensive unlabeled data also points out a new direction for alleviating site surveys. Recently, the so-called informed machine learning proposes to integrate data and prior knowledge as a hybrid information source to further enrich the information contained in the training data [20]. Specifically, a typical informed machine learning aims to solve the aforementioned problems by exploiting computer simulation results as a prominent knowledge representation [39], which is able to offer additional source of information for machine learning that goes beyond the real data. Moreover, crowdsourcing-based approaches are often employed to decompose large-scale fingerprint collection into very limited tasks to enable users to participate in [40] using heterogeneous devices. However, it is difficult to overcome the inconsistencies of fingerprints, which severely degrades the location accuracy. Therefore, it is still a challenge to find more cost-effective indoor fingerprinting localization with little site surveys.

Table. I summaries different indoor localization methods from the views of accuracy, robustness and cost-effectiveness. It is noticed that the report localization accuracy in different references cannot be compared since datasets they used are not the same. A public indoor localization dataset is required.

### B. Contributions

In this paper, we propose a novel fingerprinting localization framework based on the meta-learning [41], which is named by *MetaLoc*. It consists of three paradigms with the goal of rapid adaptation to the new environments with small-size data: i.e., vanilla model-agnostic meta-learning (MAML), model-agnostic meta-learning with task similarity (MAML-TS) and model-agnostic meta-learning with domain generalization (MAML-DG). All three paradigms aim to find the well-trained meta-parameters as the initialization to be further refined during the new environments, while their difference lies in the way they obtain the meta-parameters. Specifically, MAML-TS discovers the best environment-specific meta-parameters from the view of task similarity using maximum mean discrepancy (MMD), instead of learning one set of meta-parameters from all environments as the vanilla MAML does. In the paradigms of MAML-DG, we modify the loss function of vanilla MAML to enable the learned meta-parameters faster

convergence and better adaptation by forcing the loss on different training environments to decrease in similar directions.

In summary, the contributions of this work are three-fold:

- 1) MetaLoc is the first work to employ meta-learning for indoor localization. When facing localization tasks in a new environment, the neural network initialized by the learned meta-parameters can achieve fast adaptation against the environmental dynamics with inexpensive updates, which breaks the environment-specific localization bottleneck in a cost-effective way.
- 2) From the perspective of the models, instead of vanilla MAML, we further consider the impacts of environmental differences and propose two new paradigms, i.e., MAML-TS and MAML-DG. Theoretical analysis and experimental results are presented to prove the convergence of the proposed paradigms.
- 3) We build a public dataset to fairly compare different localization methods. The proposed MetaLoc framework is implemented from the perspective of the non-real data generated from the simulation and the real-data collected from the site survey. We design two kinds of fingerprints using wireless signal features of RSS and CSI respectively. In such design, MetaLoc can achieve adaptation with only three samples of each point in the unseen environments without significant performance degeneration.

The rest of the paper is organized as follows. Section II gives the preliminaries of the indoor localization. In Section III, we present the details of the proposed MetaLoc. The experimental setup are described in Section IV. We illustrate the performance of the proposed scheme in terms of simulation data and site survey data in Section V, while the paper is concluded in Section VI. The notations adopted throughout the paper are summarized in Table II.

## II. PRELIMINARIES

In order to verify the proposed theoretical framework, we start with RSS and CSI, which are the two mainstream signal features. Then detailed introduction of fingerprinting localization, meta-learning are the basic building blocks.

### A. Received Signal Strength (RSS)

RSS characterizes the attenuation of radio signals during propagation in decibels, which is readily accessible in the real wireless networks without additional infrastructure. However, RSS is easily vulnerable to environmental changes, which may result in fingerprints inconsistency issue. Specifically, a fingerprint could be similar to those of two or more (even far away) locations, making it impossible to distinguish fingerprints from different locations.

### B. Channel State Information (CSI)

OFDM has been widely adopted in the latest wireless techniques ranging from 802.11a, 802.11n, 802.11ac and cellular telecommunications. Different from RSS, channel response extracted from OFDM receivers can distinguish multipath characteristics in the form of channel state information (CSI). In general, CSI can be described as  $CSI = Y/X$ , where  $X$  and  $Y$  are the transmitted and received signals. The measured CSI is a complex number that can be represented by  $H_i = |H_i| e^{j \sin(\angle H_i)}$ , where  $|H_i|$  and  $\angle H_i$  represent the amplitude and phase of subcarrier  $i$ , respectively.

The most commonly used CSI collection method such as Intel 5300 CSI Tool [42] requires the successful connection to each AP. It does not work when the surrounding APs are password protected. Besides, PC-based collection methods are outdated in the current mobile Internet era. In this paper, we adopt a handy CSI collection tool based on smartphone named by Nexmon [43], which can provide more subcarrier information.

### C. Fingerprinting Localization

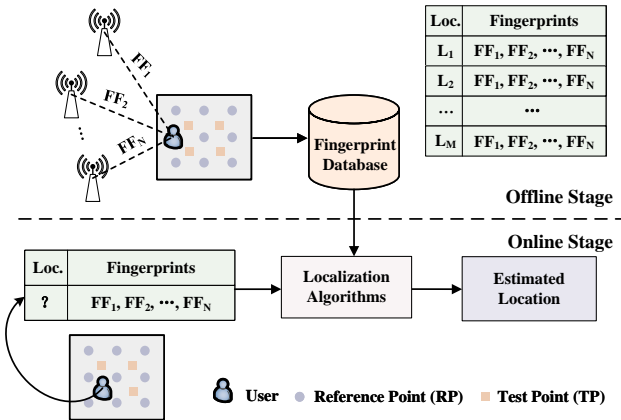


Fig. 1: Diagram of fingerprinting localization, where FF represents the fingerprint fragment collected from each AP, which can be RSS or CSI. Multiple FFs received from  $N$  APs form a fingerprint to characterize a specific position  $\mathcal{L}_i, i = 1, 2, \dots, M$ .

As shown in Fig. 1, fingerprinting localization usually consists of two stages, i.e., the offline stage and the online stage. During the offline stage, we first establish a fingerprint database, which contains the location information (abbreviated as Loc. in the figure) of the known RP and the corresponding

wireless signal measurements, such as RSS or CSI (named as fingerprints). Specifically, multiple APs are deployed in the environment as transmitters, and a walking user holds a mobile device as the receiver. Measurements from each AP can be regarded as one fingerprint fragment (FF). Multiple FFs received from  $N$  APs form a fingerprint to characterize a specific position  $\mathcal{L}_i, i = 1, 2, \dots, M$ . During the online stage, the fingerprints collected at TP with unknown locations are computed with the established fingerprint database, and some localization algorithms are used to estimate the location.

Traditionally, in the KNN algorithm, the position of each TP can be characterized by averaging its  $k$  nearest RPs in the signal space with the known physical locations. Moreover, the so-called weighted KNN (WKNN) is used when the distances are adopted as weights in the signal space. In [44], a deep learning is proposed to estimate the position of TP, which uses the neural network with random initialization and requires thousands of data to participate in the training. However, the above technologies merely focus on one specific environment and lack the ability of rapid adaptation to new and unseen environments, making massive collected data unrecyclable and wasted.

In the following, we will detail our proposed fingerprint design from the perspective of RSS and CSI.



Fig. 2: The designed fingerprint I: RSS fingerprints

1) *RSS*: From the perspective of RSS, we characterize the position of each TP in one fingerprint database by utilizing its  $k$  nearest RPs in the signal space, including the  $k$  nearest Euclidean distances and the physical coordinates of the corresponding RPs as shown in Fig. 2. Specifically,  $RSS\_dis_i, i = 1 \dots K$  represent the  $i$ -th nearest Euclidean distance between the estimated TP and all RPs in the signal space, while  $x_i, i = 1 \dots K$  represent the corresponding positions of RPs.

2) *CSI*: As shown in Fig. 3, CSI image samples are collected at two different positions in three time slots, where the gray images represent the positions of the single-channel CSI from WiFi AP0, and the colorful images represent the overlay of three-channel CSI images from three different APs, i.e., WiFi AP0, WiFi AP1, WiFi AP2. We observe that CSI images at the same location exhibit a certain similarity, and vice versa for different locations. Moreover, colorful CSI images show more stable features compared with gray images.

Furthermore, we introduce histogram intersection to compare the similarity of two different CSI images. Given a color space defined by a number of axes, the color histogram is obtained by discretizing the image colors and counting the frequency of each discrete color that occurs in the image. Thus, the colors in the image are mapped into a discrete color space containing  $n$  colors.  $Z_j(I)$  represents the frequency of color  $j$  in image  $I$ . Given a pair of histograms  $Z_j(I)$  and  $Z_j(I')$  of image  $I$  and image  $I'$  respectively, each containing  $n$  bins, the

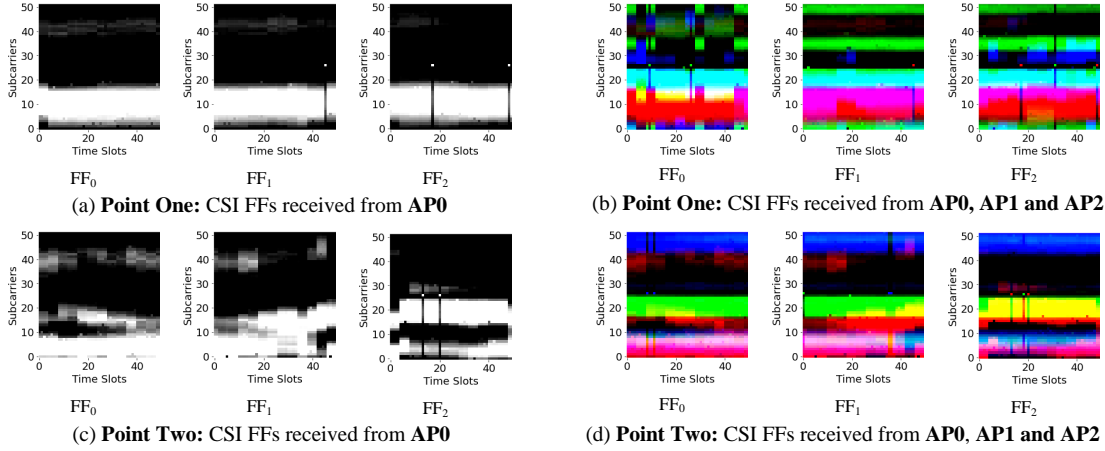


Fig. 3: The designed fingerprint II: CSI fingerprints

histogram intersection of the normalized histogram is defined as

$$Z(I) \cap Z(I') = \sum_{j=1}^n \min(Z_j(I), Z_j(I')) \quad (1)$$

For two images, the larger the value of the histogram intersection, the more similar the image pair is deemed to be. It has been extended into a metric distance as [45]

$$d(\mathbf{Z}(\mathbf{I}), \mathbf{Z}(\mathbf{I}')) = 1 - \frac{\sum_{j=1}^n \min(Z_j(I), Z_j(I'))}{\min(|\mathbf{Z}(\mathbf{I})|, |\mathbf{Z}(\mathbf{I}')|)}, \quad (2)$$

where  $\mathbf{Z}(\mathbf{I}) = [Z_1(I), \dots, Z_n(I)]$ .

#### D. Meta-learning

We briefly describe some terminologies in meta-learning framework which are the fundamentals of our proposed localization system. Meta-learning, or learning to learn, aims to observe how different machine learning approaches perform on a wide range of learning tasks, and then learn from this experience, or meta-data, to learn new tasks much faster than otherwise possible.

In meta-learning framework, tasks are assumed to be drawn from a specific distribution, i.e.,  $\tau \sim \mathcal{P}(\tau)$ , with each task containing its corresponding datasets, including training dataset (support set) and test dataset (query set). Under a  $N$ -way  $K$ -shot classification problem, a task is usually composed of  $N$  classes with  $K$  samples in each class. At meta-training stage,  $M$  tasks  $\{\tau_i\}_{i=1}^M \sim \mathcal{P}(\tau)$  are drawn from its distribution and datasets corresponding to each task are available to the agent. At meta-test stage, we are faced with a test task  $\{\tau_j\} \sim \mathcal{P}(\tau)$ , which is composed of a small training dataset and a test dataset. Meta-Learning aims to train a model using the  $M$  training tasks such that it can achieve fast adaptation on the new test task using its small training dataset, and perform well on its test dataset.

Model-Agnostic Meta-Learning (MAML) does so by learning a set of initialization  $\theta_{MAML}$  from previous training tasks, such that with only few steps of gradient descents, it can

perform well on the test task. The optimization problem of MAML at meta-training stage is formulated as:

$$\theta_{MAML} = \arg \min_{\theta} \frac{1}{M} \sum_{i=1}^M \mathcal{L}_i(\theta - \alpha \nabla_{\theta} \hat{\mathcal{L}}_i(\theta)), \quad (3)$$

where  $\mathcal{L}_i$  represents the loss function based on the dataset  $D_i$  and the inner gradient  $\nabla_{\theta} \hat{\mathcal{L}}_i(\theta)$  is based on a small mini-batch of  $D_i$ . At meta-test stage, the parameters are fine-tuned via  $\theta_j \leftarrow \theta_{MAML} - \alpha \nabla_{\theta} \hat{\mathcal{L}}_j(\theta_{MAML})$ . The detailed MAML algorithm is presented in Section III.A.

### III. THE PROPOSED SYSTEM

The goal of MetaLoc is to conduct new localization tasks as the environment changes using the neural network with only a few gradient descent steps on small-size training data. To achieve this, we train the neural network based on the fingerprint database utilizing the meta-learning algorithms. For clarity, Fig. 4 provides an overview of the proposed MetaLoc learning framework to learn localization, which comprises the meta-training and the meta-test stages. Specifically, the learned meta-parameters  $\theta^*$  derived from meta-training stage provides a warm-starting of the training process instead of learning from scratch in the meta-test stage. We explore three working paradigms of MetaLoc, including vanilla MAML, MAML-TS, and MAML-DG. The details are given below.

#### A. Vanilla MAML

In the vanilla MAML paradigm, the data collected from all environments are put together and used for the meta-training stage to obtain the meta-parameters, regardless of the environmental differences among them. The Vanilla MAML is composed of meta-training stage and meta-test stage, and the details are given below.

1) *Meta-training Stage*: We break down the meta-training process into the following three steps: i.e., initialization, inner loop and outer loop.

**Step 1: Initialization** A randomly initialized meta-parameter  $\theta$  is required to construct a neural network, represented by  $f_{\theta}$ . Besides, a distribution over tasks represented by  $\mathcal{P}(\tau)$

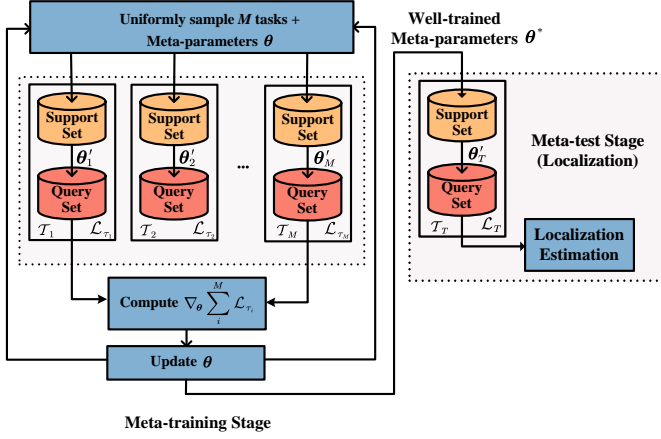


Fig. 4: The overview of the proposed MetaLoc system

is required to generate each training and test task. The task format is defined by three parameters:  $N$ -way,  $K_{spt}$ ,  $K_{qry}$ . Specifically, each localization task  $\tau_i$  is composed of  $N$  different positions with a support set  $D_{\tau_i}^s$  that contains  $K_{spt}$  number of samples and a query set  $D_{\tau_i}^q$  that contains  $K_{qry}$  number of samples under each position  $j$ , and task-specific loss functions represented by  $\mathcal{L}_{\tau_i}(f_{\theta}, D_{\tau_i}^s)$ : task-specific loss function for task  $\tau_i$  based on model parameter  $\theta$  and support set  $D_{\tau_i}^s$ ; and  $\mathcal{L}_{\tau_i}(f_{\theta}, D_{\tau_i}^q)$ : task-specific loss function for task  $\tau_i$  based on model parameter  $\theta$  and query set  $D_{\tau_i}^q$ . The underlying localization setting can be either be a classification one or a regression one. In the classification setting, the loss functions  $\mathcal{L}_i$  and  $\mathcal{L}_i$  are calculated according to cross-entropy. In regression setting, the loss functions  $\mathcal{L}_i$  and  $\mathcal{L}_i$  can either be mean-squared-error (MSE) or root-mean-square-error (RMSE).

**Step 2: Inner loop** For each localization task  $\tau_i$ , we train its own neural network model  $f_{\theta_i}$  with the support set  $D_{\tau_i}^s$  based on the initialization  $f_{\theta}$ . We obtain a task-specific parameter  $\theta'_i$  in the inner loop via one step of gradient descent, expressed as

$$\theta'_i = \theta - \alpha \nabla_{\theta} \mathcal{L}_{\tau_i}(f_{\theta}, D_{\tau_i}^s) \quad (4)$$

where the hyper-parameter  $\alpha$  represent the step size of inner loop.

**Step 3: Outer loop** After each  $\theta'_i$  is derived in Step 2, the performance of each task  $i$  can be further evaluated using its query set, given by  $\mathcal{L}_{\tau_i}(f_{\theta'_i}, D_{\tau_i}^q)$ . The sum of each specific loss across  $M$  tasks is given by  $\sum_{i=1}^M \mathcal{L}_{\tau_i}(f_{\theta'_i}, D_{\tau_i}^q)$ , which is defined as meta-loss. The goal of the outer loop is to obtain a well-trained meta-parameter  $\theta^*$  that can minimize the meta-loss, i.e.,

$$\theta^* = \arg \min_{\theta} \sum_{i=1}^M \mathcal{L}_{\tau_i}(f_{\theta}, D_{\tau_i}^q) \quad (5)$$

where  $\theta'_i = \theta - \alpha \nabla_{\theta} \mathcal{L}_{\tau_i}(f_{\theta}, D_{\tau_i}^s)$ . Note that in reality, the optimization is performed over the meta-parameter  $\theta$ , whereas the meta-loss is computed based on  $\theta'_i$ .

2) *Meta-test Stage*: After meta-training stage, we have obtained  $\theta^*$  that has absorbed the essential characteristics and differences about localization from different tasks. For a future

unseen task  $T \sim \mathcal{P}(\tau)$  which contains  $N$  different positions with support sets  $D_T^s$  and query sets  $D_T^q$ . We first initialize the neural network with  $f_{\theta^*}$ , and the task-specific adapted model parameter  $\theta'_T(Q)$  is obtained by updating  $\theta^*$  via  $Q$  steps of gradient descent on the support sets  $D_T^s$ , expressed as:

$$\theta'_T(Q) = \theta^* - \alpha \left[ \nabla_{\theta^*} \mathcal{L}_T(f_{\theta^*}; D_T^s) + \sum_{j=1}^{Q-1} \nabla_{\theta_{\tau_T(j)}} \mathcal{L}_T(f_{\theta_{\tau_T(j)}}; D_T^s) \right], \quad (6)$$

To evaluate the performance of  $\theta'_T(Q)$ , we test  $f_{\theta'_T(Q)}$  on the query set  $D_T^q$  and report the test error and localization error.

### Algorithm 1 Vanilla MAML

**Require:**  $\mathcal{P}(\tau)$ : distribution over tasks

**Require:**  $\alpha$ : inner learning rate;  $\beta$ : outer learning rate

*Meta-training Stage*

1: Randomly initialize  $\theta$

2: For *ite* in iterations do:

3: Sample  $\{\tau_i\}_{i=1}^N \sim \mathcal{P}(\tau)$

4: For *i* in range( $N$ ) do:

5:  $\theta_i = \theta - \alpha \nabla_{\theta} \mathcal{L}_{\tau_i}(f_{\theta}, D_{\tau_i}^s)$

6:  $\theta \leftarrow \theta - \beta \nabla_{\theta} \sum_{\tau_i} \mathcal{L}_{\tau_i}(f_{\theta_i}, D_{\tau_i}^q)$

7: **return**  $\theta^*$

*Meta-test Stage*

8:  $\theta_T = \theta^* - \alpha \nabla_{\theta^*} \mathcal{L}_T(f_{\theta^*}, D_T^s)$

**Summary:**

$\theta$  is updated as:

$\theta \leftarrow \theta - \beta \frac{\partial F(\cdot)}{\partial \theta}$ , where

$$F(\cdot) = \sum_{\tau_i} \mathcal{L}_{\tau_i}(f_{\theta_i}) = \sum_{i=1}^N \mathcal{L}_{\tau_i}(f_{\theta - \alpha \nabla_{\theta} \mathcal{L}_{\tau_i}}, D_{\tau_i}^q)$$

3) *Mathematical Analysis of vanilla MAML*: Here we provide analysis to answer the following two questions: (1) why is vanilla MAML able to achieve better performance than merely training a neural network with many different environments? (2) what factors affect the test performance of vanilla MAML?

Let  $T \sim \mathcal{P}(\tau)$  be any future test task with  $N$  training samples  $D_T = \{\vec{x}_i, y_i\}_{i=1}^N$ . Assume that with the well-trained initialization  $\theta^*$ ,  $m$  steps of gradient descents are implemented on  $D_T$  to obtain a fine-tuned model parameter  $\theta_T^m$ , i.e.,  $\theta_T^m = \theta^* - \alpha [\nabla_{\theta^*} \mathcal{L}_{D_T}(\theta^*) + \sum_{t=1}^{m-1} \nabla_{\theta_T^t} \mathcal{L}_{D_T}(\theta_T^t)]$ . Define the optimal parameter under task  $T$  as  $\theta_T^* = \arg \min_{\theta_T} \mathcal{L}_{\theta_T} := E_{(x,y) \sim T} [\mathcal{L}(f(\theta_T, x), y)]$ .

**Definition** (Lipschitz Continuity).  $f(\theta)$  is said to be Lipschitz continuous over a region  $D$  (bounded or unbounded) if there exists  $L > 0$  such that  $\|f(\theta_1) - f(\theta_2)\|_2 \leq L \|\theta_1 - \theta_2\|_2$  for all  $\theta_1, \theta_2 \in D$ .  $f(\theta)$  is said to be  $L$ -smooth if  $\|\nabla f(\theta_1) - \nabla f(\theta_2)\|_2 \leq L \|\theta_1 - \theta_2\|_2$ .

Next we define the loss function with respect to  $\theta_T^m$  as  $Loss(\theta_T^m) = E_{T \sim \tau} E_{D_T} [L(\theta_T^m) - L(\theta_T^*)]$ , which measures the test performance of the fine-tuned parameter  $\theta_T^m$  over  $m$  gradient steps. The lower the  $Loss(\theta_T^m)$ , the better adaptation ability the MAML possesses.

**Theorem.** Suppose  $\mathcal{L}(f(\theta, x), y)$  is  $G$ -Lipschitz continuous and  $\mathcal{L}_s$ -smooth w.r.t. the parameter  $\theta$ , and  $\alpha$  satisfies  $\alpha \leq \frac{1}{L_s}$ . Setting  $\rho = 1 + 2\alpha L$ , then for any  $T \sim \mathcal{P}(\tau)$  and  $D_T =$

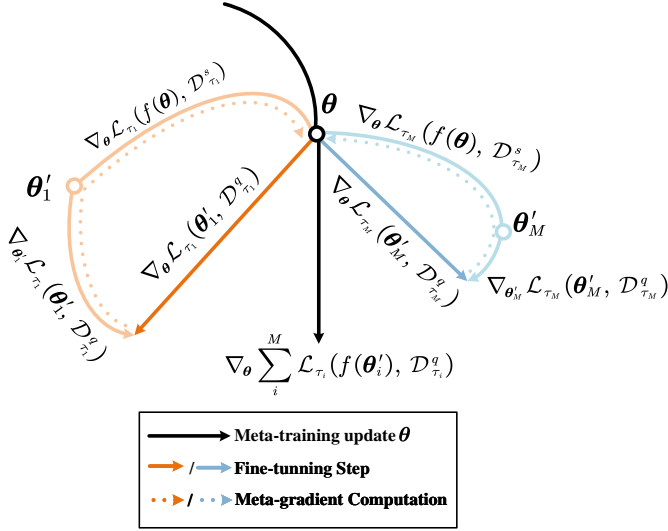


Fig. 5: Diagram of MAML, which optimizes meta-parameters  $\theta$  that can fast adapt to new tasks.

$\{\vec{x}_i, y_i\}_{i=1}^N \sim T$ , we have

$$\begin{aligned} \text{Loss}(\theta_T^m) &\leq \frac{2G^2(\rho^m - 1)}{N * L} + E_{T \sim \tau} E_{D_T} [\mathcal{L}_{D_T}(\theta_T^m) - \mathcal{L}(\theta_T^*)] \\ &\leq \frac{2G^2(\rho^m - 1)}{N * L} + \frac{1}{2\alpha} E_{T \sim \tau} [\|\theta^* - \theta_T^*\|_2^2]. \end{aligned}$$

The second inequality implies the smaller the expected distance between  $\theta^*$  and  $\theta_T^*$  over  $T$  (i.e.,  $E_{T \sim \tau} [\|\theta^* - \theta_T^*\|_2^2]$ ), the smaller the  $\text{Loss}(\theta_T^m)$  [46]. Following this idea, we compare the vanilla MAML with conventional neural network in the next.

Vanilla MAML trains the meta-parameters  $\theta$  as shown in Fig. 5, which demonstrates the paths in the parameter space with  $M$  tasks. We first conduct inner loop based on the support set of each task and obtain the task-specific parameters  $\theta'_i, i = 1, \dots, M$ . Next, outer loop is implemented to find each task's most potential direction toward the optimal parameters based on the query set. Finally, we get the direction toward the optimal parameters for each training task (in different colors), and update meta-parameters  $\theta$  based on the average across the training tasks (path in black). Thus, MAML updates  $\theta$  into a direction where all training tasks agree the most, with each  $\theta'_i$  receiving the same weight in the gradient descents of outer loop. Therefore, we expect the  $E_{T \sim \tau} [\|\theta^* - \theta_T^*\|_2^2]$  should be small in MAML. Meanwhile, there is no terminology called task, inner loop and outer loop in conventional neural network. We simply train the model using all the data of a specific dataset at one time. The issue is quite clear: the optimizer may easily overfit on a single environment by finding a descending root that achieves fast loss decrease only on this environment but with slow convergence on other environments. Under this case, we expect  $E_{T \sim \tau} [\|\theta^* - \theta_T^*\|_2^2]$  will be large. To distinguish it from meta-learning, we call this training method as joint training. The result comparisons will be shown in Section VI.

As previously mentioned, vanilla MAML only relies on a bunch of tasks from all environments but fails to consider the differences among them. In reality, the training tasks coming from different measured time or different scenarios may result in significant variations of signal features like RSS and CSI. We propose MAML-TS and MAML-DG to further deal with this issue. The former is to group different environments in advance, while the latter is to learn the differences during the meta-training stage.

## B. MAML-TS

Inspired by theorem I, the learnt meta-parameters  $\theta^*$  should be close to the optimal network parameters  $\theta_T^*$  for any task  $T$ . We propose to discover the best environment-specific meta-parameters trained from different environments of tasks in the view of task similarity, instead of learning one set of meta-parameters for all tasks. Herein we adopt maximum mean discrepancy (MMD) [47] to quantify the task similarity, which is defined as

$$\text{MMD}[\mathcal{G}, \mathcal{T}_1, \mathcal{T}_1] := \sup_{g \in \mathcal{G}} (\mathbf{E}_x[g(x)] - \mathbf{E}_y[g(y)]), \quad (7)$$

where  $x$  and  $y$  are data samples generated from the respective localization tasks  $\mathcal{T}_1$  and  $\mathcal{T}_2$  defined on space  $\mathcal{X}$ ;  $\mathcal{G}$  is a class of functions  $g : \mathcal{X} \rightarrow \mathbb{R}$ . The authors in [47] have proved that when  $\mathcal{G}$  is a unit ball in a universal reproducing kernel Hilbert space (RKHS)  $\mathcal{H}$  defined on space  $\mathcal{X}$  with associated continuous kernel,  $\text{MMD}[\mathcal{G}, \mathcal{T}_1, \mathcal{T}_1] = 0$  if and only if  $\mathcal{T}_1$  is equivalent to  $\mathcal{T}_2$ . In other words, higher MMD indicates larger difference between two tasks. Meanwhile, MMD in our experiment is conducted using several different Gaussian kernels [48].

In MAML-TS, we first cluster the training tasks into several groups, which are referred to as training environments. We train environment-specific meta-parameters instead of general meta-parameters trained on all tasks. For the target localization task, we choose its best environment-specific meta-parameters via task similarity between the test tasks and the training environments.

## C. MAML-DG

The algorithm of MAML-DG is detailed as Algorithm 2. We assume there are  $S$  domains in the training domain set  $D$ . All of them share the same label space and input features, but may have different distribution statistics. We define our deep learning model parametrized as  $\theta$ . MAML-DG aims to train  $\theta$  on all training domains such that it can be well generalized when tested on a new domain. To achieve this, in each iteration, we first randomly pick source domains  $a$  and  $b$  from the training domain set  $D$  and generate tasks in these two domains. Then in step 4 to 7, we derive a loss function  $F(\cdot)$  and virtually train a  $\theta'$  on the tasks from source domain  $a$  based on the standard MAML algorithm but  $\theta$  is not updated here. Next, with the initialization  $\theta'$ , we derive a loss function  $G(\cdot)$  on the tasks from source domain  $b$  based on the standard MAML algorithm. Finally, we sum up  $F(\cdot)$  and  $G(\cdot)$  and update the meta-parameter  $\theta$ . This is to imitate

---

**Algorithm 2** MAML-DG
 

---

**Require:**  $\{\mathcal{P}_i(\tau)\}_{i=1}^D$ : distributions over task in different domains

**Require:**  $\alpha$ : inner learning rate;  $\beta$ : outer learning rate;  $w$ : weight of the loss function of the 2nd training domain

1: Randomly initialize  $\theta$

2: For *ite* in iterations do:

3: Sample domain  $a$  and  $b$  uniformly from  $D$ .

4: Sample  $\{\tau_i^{(a)}\}_{i=1}^{N_i} \sim \mathcal{P}_a(\tau)$

5: For  $i$  in range( $N_i$ ) do:

6:  $\theta_i^{(a)} = \theta - \alpha \nabla_{\theta} \mathcal{L}_{\tau_i^{(a)}}(f_{\theta}, D_{\tau_i^{(a)}}^s)$

7:  $\theta' = \theta - \beta \nabla_{\theta} \sum_{\tau_i^{(a)}} \mathcal{L}_{\tau_i^{(a)}}(f_{\theta_i^{(a)}}, D_{\tau_i^{(a)}}^q)$

8: Sample  $\{\tau_j^{(b)}\}_{j=1}^{N_j} \sim \mathcal{P}_b(\tau)$

9: For  $j$  in range( $N_j$ ) do:

10:  $\theta_j^{(b)} = \theta' - \alpha \nabla_{\theta'} \mathcal{L}_{\tau_j^{(b)}}(f_{\theta'}, D_{\tau_j^{(b)}}^s)$

11:  $\theta \leftarrow \theta' - w * \beta \nabla_{\theta'} \sum_{\tau_j^{(b)}} \mathcal{L}_{\tau_j^{(b)}}(f_{\theta_j^{(b)}}, D_{\tau_j^{(b)}}^q)$

12: **return**  $\theta^*$

**Summary:**

$\theta$  is updated as:

$\theta \leftarrow \theta - \beta \frac{\partial(F(\cdot) + w * G(\cdot))}{\partial \theta}$ , where

$F(\cdot) = \sum_{\tau_i^{(a)}} \mathcal{L}_{\tau_i^{(a)}}(f_{\theta_i^{(a)}}) = \sum_{i=1}^{N_i} \mathcal{L}_{\tau_i^{(a)}}(f_{\theta - \alpha \nabla_{\theta} \mathcal{L}_{\tau_i^{(a)}}})$

$G(\cdot) = \sum_{\tau_j^{(b)}} \mathcal{L}_{\tau_j^{(b)}}(f_{\theta_j^{(b)}}) = \sum_{j=1}^{N_j} \mathcal{L}_{\tau_j^{(b)}}(f_{\theta' - \alpha \nabla_{\theta'} \mathcal{L}_{\tau_j^{(b)}}})$

---

the real time train-test domain shifts so that the model is able to achieve fast generalization over enough iterations.

In the indoor localization setting, the data may vary over time domains, i.e., the training and the test data may come sequentially with different measuring time. MAML-DG treats the training tasks from different time domains distinctively and thus is capable of achieving faster convergence and better performance on the test tasks that come from a new time domain.

1) *Mathematical Analysis of MAML-DG:* Here we provide mathematical analysis to help you better understand how MAML-DG works. The objective function of MAML-DG is:

$$\begin{aligned} \mathcal{L}(\theta) &= F(\theta) + w * G(\theta') \\ &= F(\theta) + w * G(\theta - \beta \nabla_{\theta} \sum_{\tau_i^{(a)}} \mathcal{L}_{\tau_i^{(a)}}(f_{\theta_i^{(a)}})) \\ &= F(\theta) + w * G(\theta - \beta * \nabla_{\theta} F(\theta)) \end{aligned} \quad (1)$$

where  $F(\theta)$  is the loss function of the first training domain, whereas  $G(\theta')$  is that of the second training domain, with  $\theta' = \theta - \beta * \nabla_{\theta} F(\theta)$  as its initialization.

With first-order Taylor's expansion, we derive that:

$$\begin{aligned} G(\theta - \beta * \nabla_{\theta} F(\theta)) &= G(\theta) + \nabla_{\theta} G(\theta) * (-\beta \nabla_{\theta} F(\theta)) \\ &= G(\theta) - \beta (\nabla_{\theta} G(\theta) \cdot \nabla_{\theta} F(\theta)) \end{aligned} \quad (2)$$

Note that the remainder of the above Taylor's expansion is:

$$\begin{aligned} R_1 &= \frac{1}{2} d^2 G(\delta) \\ &= \frac{1}{2} \{(-\beta \nabla_{\theta} F(\theta))^T \cdot \nabla_{\theta} \nabla_{\theta} G(\delta) \cdot (-\beta \nabla_{\theta} F(\theta))^T\} \end{aligned}$$

where  $\delta$  is in between  $\theta$  and  $\theta - \beta * \nabla_{\theta} F(\theta)$ .

Plug the equation (2) into (1) and our objective function becomes:

$$\begin{aligned} L(\theta) &= F(\theta) + w * G(\theta - \beta * \nabla_{\theta} F(\theta)) \\ &= F(\theta) + w * G(\theta) - w\beta (\nabla_{\theta} G(\theta) \cdot \nabla_{\theta} F(\theta)). \end{aligned} \quad (3)$$

The loss function is composed of two parts: (i)  $F(\theta) + w * G(\theta)$ , and (ii)  $-w\beta (\nabla_{\theta} G(\theta) \cdot \nabla_{\theta} F(\theta))$ . Minimizing the loss function is equivalent to minimizing both (i) and (ii). Minimizing part (i) is intuitive, which is to minimize the loss on both training domains. Next we give a detailed explanation to help you understand (ii).

Minimizing (ii) is equivalent to maximizing the dot product of  $\nabla_{\theta} G(\theta)$  and  $\nabla_{\theta} F(\theta)$ . That means, we aim to maximize  $\|\nabla_{\theta} F(\theta)\|_2 \cdot \|\nabla_{\theta} G(\theta)\|_2 \cdot \cos(\delta)$ , where  $\delta$  represents the angle between  $\nabla_{\theta} F(\theta)$  and  $\nabla_{\theta} G(\theta)$ . Therefore, the dot product is larger if  $\nabla_{\theta} F(\theta)$  and  $\nabla_{\theta} G(\theta)$  tend to tilt in the same direction.

Combining (i) and (ii) together, the optimizer aims to *optimize such that the losses of both training domains are minimized in a similar direction*. For the generally used objective function  $F(\theta) + G(\theta)$ , the optimizer may easily overfit on a single domain by finding a descending root that achieves fast decrease only on one domain but with slow convergence on the other domain. Therefore, compared to MAML, MAML-DG is capable of alleviating overfitting and achieves good generalization ability among different training domains.

#### IV. EXPERIMENTAL SETUP

In this section, we describe our experimental environments and the devices for collecting CSI and RSS from the perspective of (A) non-real data in the simulation and (B) real-data in the site surveys. Specifically, simulation provide non-real data for the toy examples to demonstrate the convergence of the proposed MetaLoc. After that, we conduct the more practical experiments based on the real data in the site surveys.

##### A. Non-Real Data in Simulation

In wireless communication, electromagnetic wave strength decays with the increase of propagation distance. We separate communication links as Line-of-sight (LOS) and non-line-of-sight (NLOS), whose probabilities fit the propagation are given in Eq. (1) of [49] citing the 3GPP specification. We consider multiple path-loss models that have been validated by extensive measurement campaigns to capture the signal propagation property of various indoor environments, including: **Model (a) vanilla log-distance model**, see Eq. (1) of [50]; **Model (b) shopping malls with NLOS dual slope**, see Eq. (7) of [49]; **Model (c) office with LOS and NLOS single slope** [51]; **Model (d) office with a frequency-dependent path loss**



TABLE III: Localization Results

Methods	Hall		Lab	
	Mean errors (m)	Std (m)	Mean errors (m)	Std (m)
MAML	2.11	1.17	3.10	1.43
MAML-DG	2.07	1.11	3.04	1.39
MAML-TS	2.09	1.18	3.09	1.35
JT	2.27	1.27	3.97	1.99
RI	2.59	1.29	4.19	1.95
ConFi	2.89	0.48	3.53	0.47
ILCL	3.61	2.06	3.48	1.62
KNN	2.73	1.35	3.35	1.42

**exponent**, see Eq. (2) and Eq. (5) of [49]; **Model (e) shopping malls with LOS and NLOS dual slope**, see Eq. (2) and Eq. (8) in [49].

We randomly deploy 24 APs operating at 2440 MHz as transmitters. The number of RPs ranges from 10 to 54. For datasets, each TP is set to be characterized by its 5 nearest RPs in the signal space. We assume that the number of support samples is 100 and the number of query samples is 30 for each task.

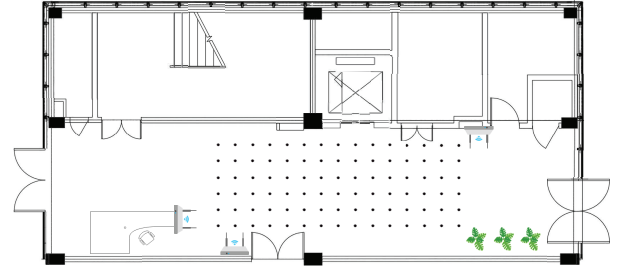
To test the performance of MetaLoc, we utilize the vanilla log-distance path-loss model operating at different standard deviation (std) to generate simulation data with the experimental settings given in Table I of reference [1].

To test the impact of environment-specific meta-parameters, instead of the vanilla log-distance model, we select multiple path-loss models in 3GPP to characterize practical scenarios. Table II in [1] lists training tasks with various transmit power, scenario size, and noise. We divide them into three different environments based on the generation of path loss models, that is, Env. One is generated from **Model (b)**, Env. Two is from **Model (c)** and Env. Three is from **Model (d)**. Meanwhile, the test tasks are simulated in the scenarios with constant shape size  $10\text{ m} \times 10\text{ m}$  and transmit power  $P_t = 10\text{ dBm}$ . Specifically, Test Task One is simulated from **Model (e)** with  $\sigma_{LOS} = 3$ ,  $\sigma_{NLOS} = 6.26$ ; Test Task Two and Three are generated from **Model (b)** with  $\sigma_{NLOS} = 5$  and  $\sigma_{NLOS} = 15$  respectively. Note that these two models both simulate scenarios of shopping malls. MMD measures the average difference between each test task and the training environments, as shown in Fig. 9.

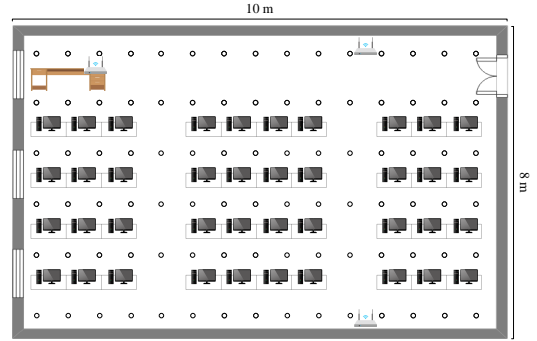
## B. Site Surveys

1) *Devices*: We implement MetaLoc using three different types of routers as the transmitters, i.e., ASUS RT-AC86U, TPlink TL-WR885N, and TPlink TL-WR886N. Mobile phone Nexus 5 acts as the receiver. The whole system works at 5 GHz with a bandwidth of 20 MHz to ensure the higher channel quality.

2) *Scenarios*: We conduct our experiments in two different scenarios: i.e., hall and lab in the CUHKSZ. Specifically, as shown in Fig. 6 (a), the hall with the area of  $12\text{ m} \times 5\text{ m}$  is complex as people walk around when CSI fingerprints are collected, resulting in noise to the data. Other than the passers-by from time to time, the test area is almost empty and can be regarded as a Line-of-Sight (LOS) area. We uniformly select 90 points for data-collection, where the distance is 0.6



(a) Hall of Letian Building in CUHKSZ



(b) Lab in CUHKSZ

Fig. 6: Two different experimental scenarios in the site surveys

m between each two adjacent points. Data are collected once a week for five times in the hall. Then we set up our test facilities in a  $10\text{ m} \times 8\text{ m}$  lab room, as shown in Fig. 6 (b). The environment of the test area is rather complicated as there are lots of obstacles such as desks and machines in the room. The test site  $B$  can be regarded as a None-Line-of-Sight (NLOS) area. We select 90 points for data-collection, distributed in a  $10\text{ m} \times 8\text{ m}$  rectangular area. Different from hall, the resolution of fingerprints in lab is not uniform. Specifically, the interval between two points is 0.6 m or 1.2 m. Data are collected once a week for five times in the lab.

## C. Comparison Methods

We implement MetaLoc framework in the CNN model including five convolution layers, pooling layers and a fully-connected layer. We compare the proposed framework with test Joint Training, Random Initialization, KNN, ILCL, and ConFi on the site survey data. The details are as follows: In the KNN model, We set  $K$  as 5, pick out each TP's five closest RPs, treat their averaged coordinate as the predicted coordinate, and finally report the localization error. In the Joint Training model, instead of following the standard procedures of Meta-Training in MAML, we adopt the traditional stochastic gradient descent (SGD) method to train the CNN model and obtain the best model parameters as the initialization, and then fine-tune the model and report the localization error for each test task as in meta-test stage. In the Random Initialization model, we randomly generate a set of CNN parameters and use that as the initialization of meta-test stage. The test tasks' format and the hyper-parameters of Joint Training and Random

Initialization in meta-test stage are exactly the same as those in MAML, MAML-DG, and MAML-TS. In the ILCL model, we set the number of incremental steps  $L$  of BLS classification regression as 10, while other hyper-parameters are set as default. In ConFi, the structure of the neural network and the dataset involved in the procedure of training and test are set to be the same as the MAML used, but the data no longer exists in the form of tasks.

## V. EXPERIMENTAL EVALUATION

In this section, we will present the preliminary results of MetaLoc’s cross-environment adaptation abilities based on the simulated data, and the cross-environment adaptation abilities of MAML, MAML-TS, and MAML-DG based on the real site-surveyed data collected from *Scenario A* and *Scenario B*.

In the following, we will fully verify the efficacy of the proposed MetaLoc from two perspectives, i.e., easier-to-implement simulation data and more realistic site survey data.

### A. Preliminary Results Based on Simulation Data

1) *Convergence*: To observe a rough view on the performance of cross-space adaptation abilities of MetaLoc, we first test it on the simulation data together with the traditional KNN and WKNN models. The relationship between RMSE and the number of gradient steps versus the training data size is illustrated in Fig. 7. The red curve shows that MetaLoc converges much faster than those non-MetaLoc methods that are trained using the same neural network architecture but with random initialization of the network parameters.

Moreover, the performance of the non-MetaLoc is primarily affected by the training data size, i.e., non-MetaLoc performance improves with an increasing size. When the data size rises to 8000, the localization performance becomes saturated, reaching a level slightly inferior that of MetaLoc, but the latter merely requires 124 data for training. Compared with the traditional fingerprinting methods that strongly rely on the large amount of data collected in the target scenario, MetaLoc framework exploits the existing database built for a batch of different scenarios.

2) *Localization error*: We sample 1000 test samples randomly in the test task and quantify the localization errors in terms of the cumulative distribution function (CDF). Fig. 8 presents the CDF of the localization error versus different numbers of RPs ( $N$ ), where  $N = 10, 20, 30, 40, 54$ . We observe that more RPs deployed in the scenario can promote localization accuracy due to abundant characteristics of the multipath channel fed into network. More specifically, when  $N = 54$ , the localization results of traditional KNN, WKNN and our MetaLoc are nearly the same. While as  $N$  decreases, the performance gap becomes larger, and MetaLoc shows higher resistance to performance degradation. When  $N$  decreases to 10, the probability of localization errors of MetaLoc, WKNN, KNN being less than 5 m are 0.89, 0.65, 0.51, respectively. MetaLoc presents better accuracy in the harsh case of  $N = 10$ . The above findings indicate that MetaLoc reduces the dependence on big amount of RPs and shows the best cost-effectiveness in constructing fingerprint database.

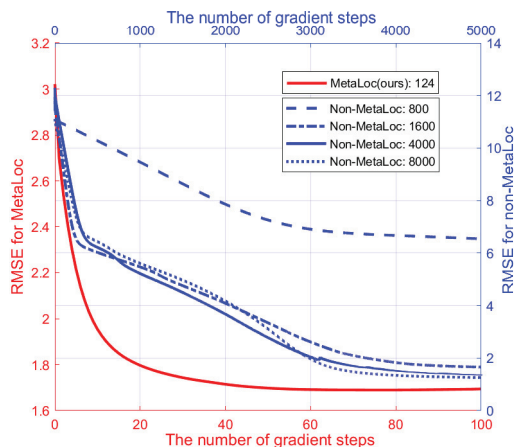


Fig. 7: RMSE convergence comparisons between MetaLoc and non-MetaLoc, in which data are generated from Model (a) vanilla log-distance model. In the double-axis system, the red-axis system represents MetaLoc with 124 training data while the blue-axis system represents non-MetaLoc with 8000, 4000, 1600, 800 training data, respectively.

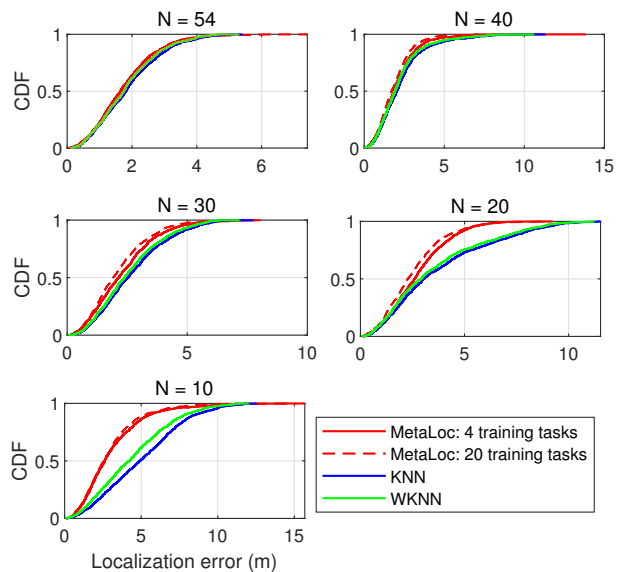


Fig. 8: CDFs of localization errors (m) under different numbers of RPs ( $N$ ).

3) *Impact of environment-specific meta-parameters*: In Fig. 9,  $\theta_1$ ,  $\theta_2$  represent environment-specific meta-parameters trained on Env. One and Env. Two, and  $\theta_{total}$  are trained on all three environments listed in Table II of reference [1]. First of all, we observe that MMD can reflect the quality of the test performance. Specifically, the test tasks with smaller MMD values present better localization results. Secondly, the learned meta-parameters achieve rapid convergence on multiple test tasks, showing good generalization ability to new scenarios. Besides, in test tasks with common noise std proposed in 3GPP, environment-specific meta-parameters  $\theta_1$  present better

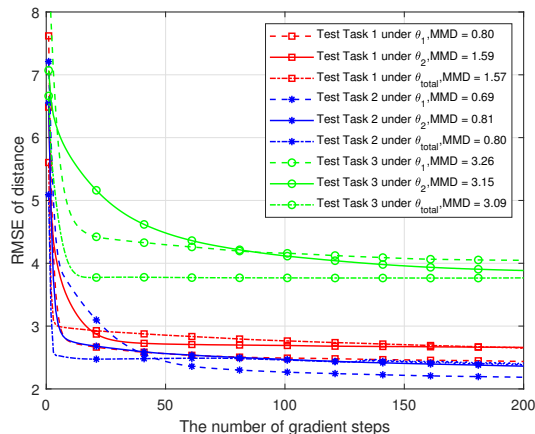


Fig. 9: The test results comparison among three different meta-parameters, where  $\theta_1$ ,  $\theta_2$ ,  $\theta_{total}$  represent well-trained meta-parameters based on Env. One, Env. Two, and total training tasks listed in Table II of reference [1], respectively.

results compared with  $\theta_2$  and  $\theta_{total}$ . The reason is that Env. Two and Env. Three, both generated from office scenarios, cannot provide much specific assistance for these test tasks simulated in malls and even may introduce outliers. However, as the noise std added to test tasks becomes significantly large, there is no obvious improvement of test tasks on  $\theta_1$ , which exists limitation in special cases with extreme noise std input. Overall, the above results indicate that MMD can provide prior information about task similarity for test tasks to assist the selection of environment-specific meta-parameters and further facilitate localization accuracy.

4) *Wireless Insite (WI)*: WI is a suite of ray-tracing models developed by REMCOM. It can simulate and predict the complex space using advanced electromagnetic processing methods. Compared with path loss models, WI can generate scenarios realistically and provide more reliable data. Then, we conduct the experiments under data sets generated by WI platform shown in the supplementary files. Scenario 1, 2, 5, 6 are chosen as training tasks and Scenario 3, 4 are chosen as testing tasks. Fig. 10 compares RMSE results for data generated from WI platform under well-trained parameters obtained by the proposed system. Results are convergent extremely fast in 50 iterations under four scenarios. Interestingly, solid lines are observed to be convergent more quickly than dot lines. A possible explanation for this might be that well-trained initialization from path loss models (abbreviated as PLM in the figure) and WI would have more knowledge of channel features than those trained only over WI data. The findings show that simulation data may can provide extra support and motivate us to solve data-hungry issues in the real localization environments.

### B. Localization Results Based on Site Survey Data

After witnessing the good performance of vanilla MAML and environment-specific meta-parameters on the simulated data, here we present more comprehensive results to demonstrate the cross-environment adaptation abilities of vanilla

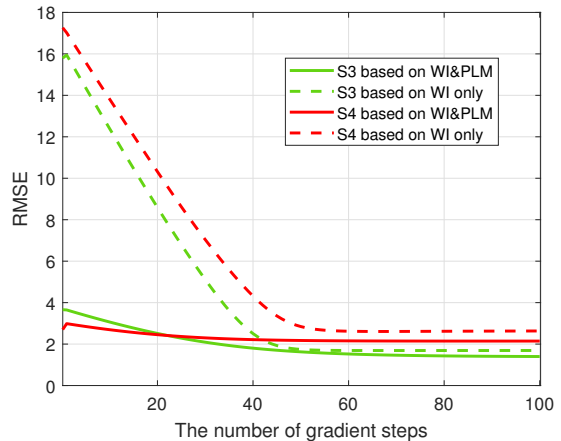


Fig. 10: Comparison results for data generated from WI platform

MAML, the proposed MAML-DG, and MAML-TS based on the real site survey data.

As for the training procedure, we set  $N = 10$ ,  $K_{spt} = 3$ ,  $K_{qry} = 5$  as the training task format. Besides, we set the inner learning rate to be  $\alpha = 0.01$  and the outer learning rate to be  $\beta = 0.001$  for MAML, MAML-DG, and MAML-TS. In addition, we set the iteration steps as 7500, the task-level inner update steps (i.e., the number of gradient descent steps for inner loop of each task in *Meta-Training* stage) as 5, the outer update step as 1, and the number of gradient descent steps of fine-tuning in *Meta-Test* stage as 10.

There are two types of errors to be reported for MAML, MAML-DG, MAML-TS, Joint Training, and Random Initialization: (1) *Test Error (with respect to Q)*: Averaged test errors on query sets of test task with respect to the number of gradient steps  $Q$  of fine-tuning; (2) *Localization Error*: Prediction error for each test point (TP). For all other models in comparison, we will only report the averaged localization error.

In this section, we will present the averaged localization errors and cumulative density functions (CDFs) of localization errors for MAML, MAML-DG, MAML-TS, Joint Training, Random Initialization, KNN, ConFi and ILCL shifted from dynamic environments. Besides, we will also present the comparisons between MAML, MAML-DG, and MAML-TS regarding test error with respect to the number of gradient steps in fine-tuning during meta-test stage, and the comparisons between MAML, MAML-DG, MAML-TS, Joint Training, and Random Initialization regarding localization error with respect to the number of iterative steps of Outer loop. The reported localization error is the averaged localization errors on all the tested environments. We apply the similar training and test settings for ILCL and ConFi, i.e., the two models are trained on sufficient data from all other environments and then are fine-tuned on the test environment with only a small amount of data. The detailed training and test procedures are detailed below.

To test MAML or MAML-DG on the test environment  $k$ , we first train the model on tasks generated from data on all other environments other than environment  $k$ . After that, we

collect nine CSI images (1 for choice of RPs, 3 for fine-tuning and 5 for test) on each point in the test environment  $k$  during meta-test stage. And then, we construct our test tasks in the following way. For each TP  $i$ , we collect only one CSI image of it, and then adopt the histogram intersection method to select its 5 nearest RPs. Specifically, we calculate the similarity using Eq. (2) between point  $i$ 's CSI image and each RP's pre-collected one CSI image, and then pick out 5 RPs whose CSIs are the closest to  $i$ 's. Next, we form a test task  $T$  composed of these  $K$  RPs with each support set containing 3 CSI images and each query set containing the other 5 CSI images. Finally, to test on task  $T$ , we first fine-tune our model using support sets of  $T$ , and then predict and derive the localization error  $e_{i,k}^{loc}$  of the  $i$ -th TP on environment  $k$ , and report the average localization error  $error_k^{loc} = \frac{\sum_{i=1}^{90} e_{i,k}^{loc}}{90}$ . The final reported localization error is  $\frac{\sum_{k=1}^N error_k^{loc}}{N}$ . Besides, we will also report the averaged test errors with respect to the number of gradient steps of fine-tuning in the meta-test stage. Specifically, we test  $f_{\theta_T^*}(Q)$  on the query set  $\{D_{T,j}^q\}_{j=1}^N$  and obtain the test errors  $\{e_{T,j}^{test}(Q)\}_{j=1}^N$  with respect to the number of gradient steps  $Q$ . And the averaged test error is reported as  $error_T^{test}(Q) = \frac{\sum_{j=1}^N e_{T,j}^{test}(Q)}{N}$  for  $Q$  ranging from 0 to 10.

To test the efficacy of MAML-TS, we assume that the environment on date  $d$  is the test environment that we will adapt to, while environments on other dates are regarded as the training environments. Firstly, we use Eq. 7 to measure the difference between data collected on the test environment and training environments. The meta-parameters of the environment where the calculated MMD is smallest will be selected as the optimal meta-parameters to involve in the adaptation in the unseen test environment. The generation of test task for MAML-TS is exactly the same as that for MAML and MAML-DG.

1) *Localization Errors*: Fig. 11 demonstrate the CDFs of localization errors of MAML, MAML-DG, MAML-TS, Joint Training, Random Initialization, ConFi, ILCL, and KNN under their corresponding optimal hyper-parameters and optimal training steps. We observe that the CDFs of MAML, MAML-TS, and MAML-DG are very similar, implying that their post-trained meta-parameters are close to each other. Besides, CDFs of MAML, MAML-TS, and MAML-DG present the better localization performance among other popular localization models. Furthermore, the averaged localization errors and corresponding standard deviations (std) of different models in the hall and the lab are shown in Table. III. The performance of the vanilla MAML paradigm is significantly better than all other models, with a mean error that is around 2.10 m in the hall and 3.10 m in the lab. The MAML-DG and MAML-TS can achieve slightly better localization performance than MAML. The more detailed comparisons with other test models will be given in the Section V-B4.

2) *Convergence of Test Errors*: Fig. 12 presents the convergence results of test errors  $error_T^{test}(Q)$  with respect to the number of gradient steps  $Q$  during meta-test stage. The figure demonstrates that compared to the joint training which adopts standard SGD during training process, and random initialization which randomly generates a set of parameters directly used for fine-tuning, the vanilla MAML, MAML-DG,

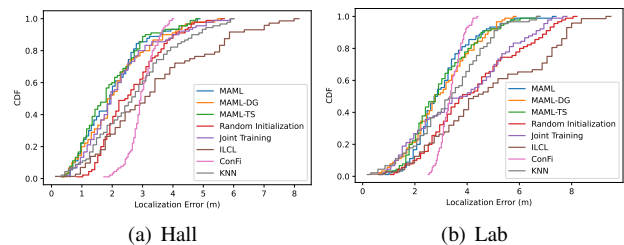


Fig. 11: CDF comparison of localization errors

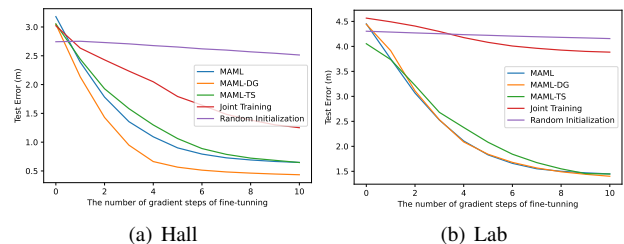


Fig. 12: Test error convergence

and MAML-TS only require a few gradient steps (around 4-6) to achieve satisfactory performance during meta-test stage, showcasing their great adaptation abilities in the environmental dynamics. Moreover, Fig. 12 clearly shows that MAML-DG is able to achieve even faster adaptation abilities than MAML and MAML-TS, and few less gradient steps are required to converge. This is as expected since MAML-DG is designed to capture the domain differences and achieve faster convergence on a new time domain. However, MAML-TS's error convergence is inferior to MAML and MAML-DG. As mentioned above, MAML-TS only selects the data of one environment for training, which reduces the amount of training data but may have the overfitting issue.

3) *Convergence of Localization Errors*: Localization errors with respect to the number of iterative steps of outer loop for MAML, MAML-DG, and MAML-TS is shown in Fig. 13. Overall speaking, MAML-TS and MAML-DG can achieve faster convergence and smaller localization error than MAML, while MAML-DG's performance is significantly better. We can see that sometimes the convergence results of MAML-TS are less satisfactory. This phenomenon is probably out of overfitting, as each MAML model in MAML-TS is only trained on one specific environment as we mentioned before.

4) *Conclusions and Comparisons*: In conclusion, MAML, MAML-DG, and MAML-TS can achieve very satisfactory cross-environment adaptation abilities on test tasks with only small amount of localization data. MAML-DG and MAML-TS can achieve faster convergence and smaller localization errors than MAML in most cases. The advantage of MAML-DG over MAML is significant, while MAML-TS sometimes may have inferior performance originated from overfitting issues. Compared to the standard joint training method, MetaLoc is superior in terms of much better localization error and significantly faster convergence (much less gradient steps of fine-tuning are required for MetaLoc).

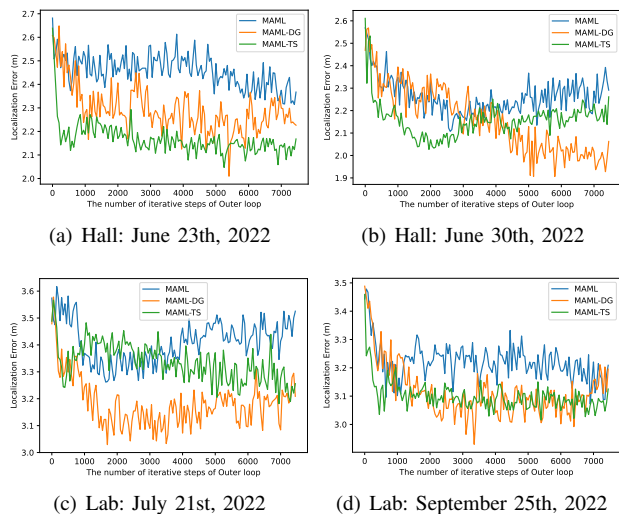


Fig. 13: Convergence comparison of localization errors in the hall and lab

ILCL model is susceptible to data change and tends to overfit when the number of samples of each test point is small. Tested on our data, under the same set of model parameters, if we slightly change the number of CSI images of each test point, then the average localization error will be changed significantly. For example, if we fix the regularization term  $L$  as  $2 \times 10^{-7}$  in the BLS classification regression during the test step and test the model on each test point with one or two CSI images, the average localization errors will be 2.41m and 4.50m, respectively. After the parameters are adjusted to the optimal under each situation, through the test results, we find that if the number of CSI images of each test point is less than 3, the model tends to overfit severely as indicated by the standard deviations. Compared to ILCL, our model is more robust and can adapt to each test scenario quickly with only small sample size.

ConFi is the first model to invoke CNN for indoor localization. However, the model lacks consideration for environmental changes. As indicated by Table III, the mean localization error of ConFi is around 2.9 m in LOS room and 3.5m in NLOS room, which is even slightly higher than the simple KNN model. But ConFi is advantageous at its lowest variance among all the tested models, meaning that the model is capable of achieving a stable performance. However, the model is less likely to give an accurate prediction for any TP, as the lowest localization error that can be achieved by ConFi is as high as 1.8 m, while others can be as low as 0.1 m.

KNN is a standard and typical model used for indoor localization. As shown in Table III, the mean localization error of KNN is around 3.2 m, and the variance of it is high, which present the unstable performance. This is as expected since KNN has the poor tolerance to the outliers, while the real indoor environment is changeable, and abnormal values are prone to occur, which beyond the ability of KNN.

## VI. CONCLUSION

To enhance the traditional environment-specific localization methods, MetaLoc has been designed in this paper to explore a fast adaptive fingerprinting localization using fewer data samples. Empowered by meta-learning, fingerprint database established in the past can be reused to serve new localization tasks in the new environments. Experimental results demonstrate the efficacy of rapid adaptation to new environments and good generalization ability of MetaLoc. The proposed paradigms of MAML-TS and MAML-DG in MetaLoc present better convergence performance due to considering the impact of environmental differences.

## REFERENCES

- [1] J. Gao, C. Zhang, Q. Kong, F. Yin, L. Xu, and K. Niu, "Metaloc: Learning to learn indoor RSS fingerprinting localization over multiple scenarios," in *Proc. IEEE Int. Conf. Commun. (ICC)*, May 2022, pp. 3232–3237.
- [2] R. Faragher and R. Harle, "Location fingerprinting with bluetooth low energy beacons," *IEEE J. Sel. Areas Commun.*, vol. 33, no. 11, pp. 2418–2428, 2015.
- [3] M. Youssef and A. Agrawala, "The Horus WLAN location determination system," in *Proc. Int. Conf. Mobile Syst. Appl. Serv. (MobiSys)*, 2005, pp. 205–218.
- [4] F. Yin, C. Fritsche, F. Gustafsson, and A. M. Zoubir, "TOA-based robust wireless geolocation and cramer-rao lower bound analysis in harsh LOS/NLOS environments," *IEEE Trans. Signal Process.*, vol. 61, no. 9, pp. 2243–2255, 2013.
- [5] H. Godrich, A. M. Haimovich, and R. S. Blum, "Target localization accuracy gain in mimo radar-based systems," *IEEE Trans. Inf. Theory*, vol. 56, no. 6, pp. 2783–2803, 2010.
- [6] G. Bresson, Z. Alsayed, L. Yu, and S. Glaser, "Simultaneous localization and mapping: A survey of current trends in autonomous driving," *IEEE Trans. Intell. Transp. Syst.*, vol. 2, no. 3, pp. 194–220, 2017.
- [7] R. Wei, B. Li, H. Mo, B. Lu, Y. Long, B. Yang, Q. Dou, Y. Liu, and D. Sun, "Stereo dense scene reconstruction and accurate localization for learning-based navigation of laparoscope in minimally invasive surgery," *IEEE. Trans. Biomed. Eng.*, 2022.
- [8] S. Jeong, S. Kuk, and H. Kim, "A smartphone magnetometer-based diagnostic test for automatic contact tracing in infectious disease epidemics," *IEEE Access*, vol. 7, pp. 20734–20747, 2019.
- [9] B. Zhou, A. Liu, and V. Lau, "Successive localization and beamforming in 5G mmWave MIMO communication systems," *IEEE Trans. Signal Process.*, vol. 67, no. 6, pp. 1620–1635, 2019.
- [10] J. Gante, G. Falcao, and L. Sousa, "Deep learning architectures for accurate millimeter wave positioning in 5G," *Neural Process. Lett.*, vol. 51, no. 1, pp. 487–514, 2020.
- [11] Z. Wang, Z. Liu, Y. Shen, A. Conti, and M. Z. Win, "Location awareness in beyond 5g networks via reconfigurable intelligent surfaces," *IEEE J. Sel. Areas Commun.*, 2022.
- [12] F. Zafari, A. Gkelias, and K. K. Leung, "A survey of indoor localization systems and technologies," *IEEE Commun. Surv. Tutor.*, vol. 21, no. 3, pp. 2568–2599, 2019.
- [13] S. Ali, W. Saad, N. Rajatheva, K. Chang, D. Steinbach, B. Sliwa, C. Wietfeld, K. Mei, H. Shiri, H.-J. Zepernick *et al.*, "6G white paper on machine learning in wireless communication networks," *arXiv preprint arXiv:2004.13875*, 2020.
- [14] P. Bahl and V. N. Padmanabhan, "RADAR: An in-building RF-based user location and tracking system," in *Proc. IEEE Int. Conf. Comput. Commun. (INFOCOM)*, vol. 2, 2000, pp. 775–784.
- [15] C.-H. Hsieh, J.-Y. Chen, and B.-H. Nien, "Deep learning-based indoor localization using received signal strength and channel state information," *IEEE Access*, vol. 7, pp. 33256–33267, 2019.
- [16] F. Yin and F. Gunnarsson, "Distributed recursive Gaussian processes for RSS map applied to target tracking," *IEEE J. Sel. Top. Sign. Proces.*, vol. 11, no. 3, pp. 492–503, 2017.
- [17] D. Jin, F. Yin, C. Fritsche, F. Gustafsson, and A. M. Zoubir, "Bayesian cooperative localization using received signal strength with unknown path loss exponent: Message passing approaches," *IEEE Trans. Signal Process.*, vol. 68, pp. 1120–1135, 2020.

- [18] R. S. Sinha, S.-M. Lee, M. Rim, and S.-H. Hwang, "Data augmentation schemes for deep learning in an indoor positioning application," *Electronics*, vol. 8, no. 5, p. 554, 2019.
- [19] A. Shrivastava, T. Pfister, O. Tuzel, J. Susskind, W. Wang, and R. Webb, "Learning from simulated and unsupervised images through adversarial training," in *Proc. IEEE Conf. Comput. Vis. Pattern Recognit.(CVPR)*, 2017, pp. 2107–2116.
- [20] L. von Rueden, S. Mayer, K. Beckh, B. Georgiev, S. Giesselbach, R. Heese, B. Kirsch, J. Pfrommer, A. Pick, R. Ramamurthy *et al.*, "Informed machine learning—a taxonomy and survey of integrating knowledge into learning systems," *arXiv preprint arXiv:1903.12394*, 2019.
- [21] F. Yin, Y. Zhao, F. Gunnarsson, and F. Gustafsson, "Received-signal-strength threshold optimization using Gaussian processes," *IEEE Trans. Signal Process.*, vol. 65, no. 8, pp. 2164–2177, 2017.
- [22] J. Torres-Sospedra, R. Montoliu, A. Martínez-Usó, J. P. Avariento, T. J. Arnau, M. Benedito-Bordonau, and J. Huerta, "UJIIndoorLoc: A new multi-building and multi-floor database for WLAN fingerprint-based indoor localization problems," in *Proc. IEEE Int. Conf. Indoor Position. Indoor Navig. (IPIN)*, 2014, pp. 261–270.
- [23] K. Wu, J. Xiao, Y. Yi, M. Gao, and L. M. Ni, "Fila: Fine-grained indoor localization," in *Proc. IEEE Int. Conf. Comput. Commun. (INFOCOM)*, IEEE, 2012, pp. 2210–2218.
- [24] X. Wang, L. Gao, S. Mao, and S. Pandey, "DeepFi: Deep learning for indoor fingerprinting using channel state information," in *Proc. IEEE Wireless Commun. and Netw. Conf. (WCNC)*, 2015, pp. 1666–1671.
- [25] X. Wang, X. Wang, and S. Mao, "CiFi: Deep convolutional neural networks for indoor localization with 5 GHz Wi-Fi," in *Proc. IEEE Int. Conf. Commun. (ICC)*, 2017, pp. 4673–4999.
- [26] H. Chen, Y. Zhang, W. Li, X. Tao, and P. Zhang, "ConFi: Convolutional neural networks based indoor wi-fi localization using channel state information," *IEEE Access*, vol. 5, pp. 18 066–18 074, 2017.
- [27] Z. Gao, Y. Gao, S. Wang, D. Li, and Y. Xu, "CRISLoc: Reconstructable CSI fingerprinting for indoor smartphone localization," *IEEE Internet Things J.*, pp. 3422–3437, 2021.
- [28] L. Li, X. Guo, M. Zhao, H. Li, and N. Ansari, "TransLoc: A heterogeneous knowledge transfer framework for fingerprint-based indoor localization," *IEEE Trans. Wireless Commun.*, vol. 20, no. 6, pp. 3628–3642, 2021.
- [29] C. Wu, J. Xu, Z. Yang, N. D. Lane, and Z. Yin, "Gain without pain: Accurate wifi-based localization using fingerprint spatial gradient," *Proc. ACM on Interactive, Mobile, Wearable and Ubiquitous Technologies (IMWUT)*, vol. 1, no. 2, pp. 1–19, 2017.
- [30] C. Wu, Z. Yang, C. Xiao, C. Yang, Y. Liu, and M. Liu, "Static power of mobile devices: Self-updating radio maps for wireless indoor localization," in *Proc. IEEE Int. Conf. Comput. Commun. (INFOCOM)*, 2015, pp. 2497–2505.
- [31] X. Chen, H. Li, C. Zhou, X. Liu, D. Wu, and G. Dudek, "Fidora: Robust wifi-based indoor localization via unsupervised domain adaptation," *IEEE Internet Things J.*, 2022.
- [32] H. Li, X. Chen, J. Wang, D. Wu, and X. Liu, "Dafi: Wifi-based device-free indoor localization via domain adaptation," *Proc. ACM on Interactive, Mobile, Wearable and Ubiquitous Technologies (IMWUT)*, vol. 5, no. 4, pp. 1–21, 2021.
- [33] S.-H. Fang and C.-H. Wang, "A novel fused positioning feature for handling heterogeneous hardware problem," *IEEE Trans. Commun.*, vol. 63, no. 7, pp. 2713–2723, 2015.
- [34] X. Zhu, W. Qu, X. Zhou, L. Zhao, Z. Ning, and T. Qiu, "Intelligent fingerprint-based localization scheme using csi images for internet of things," *IEEE Trans. Netw. Sci. Eng.*, 2022.
- [35] S. He and S.-H. G. Chan, "Sectjunction: Wi-Fi indoor localization based on junction of signal sectors," in *Proc. IEEE Int. Conf. Commun. (ICC)*, IEEE, 2014, pp. 2605–2610.
- [36] Y. Jiang, X. Pan, K. Li, Q. Lv, R. P. Dick, M. Hannigan, and L. Shang, "Ariel: Automatic Wi-Fi based room fingerprinting for indoor localization," in *Proc. ACM UbiComp*, 2012, pp. 441–450.
- [37] C.-L. Wu, L.-C. Fu, and F.-L. Lian, "Wlan location determination in e-home via support vector classification," in *IEEE Int. Conf. Netw. Sens. and Control(Proc. IEEE ICNSC)*, 2004, vol. 2. IEEE, 2004, pp. 1026–1031.
- [38] G. Nuno-Barrau and J. M. Páez-Borrillo, "A new location estimation system for wireless networks based on linear discriminant functions and hidden Markov models," *EURASIP J. Appl. Signal Process.*, vol. 2006, pp. 1–17, 2006.
- [39] T. M. Deist, A. Patti, Z. Wang, D. Krane, T. Sorenson, and D. Craft, "Simulation-assisted machine learning," *Bioinf.*, vol. 35, no. 20, pp. 4072–4080, 2019.
- [40] S. Yang, P. Dessai, M. Verma, and M. Gerla, "FreeLoc: Calibration-free crowdsourced indoor localization," in *Proc. IEEE Int. Conf. Comput. Commun. (INFOCOM)*, 2013, pp. 2481–2489.
- [41] C. Finn, P. Abbeel, and S. Levine, "Model-agnostic meta-learning for fast adaptation of deep networks," in *Proc. Int. Conf. Mach. Learn.*, 2017, pp. 1126–1135.
- [42] D. Halperin, W. Hu, A. Sheth, and D. Wetherall, "Tool release: Gathering 802.11 n traces with channel state information," *ACM SIGCOMM computer communication review*, vol. 41, no. 1, pp. 53–53, 2011.
- [43] M. Schulz, D. Wegemer, and M. Hollick. (2017) Nexmon: The c-based firmware patching framework. [Online]. Available: <https://nexmon.org>
- [44] R. P. Ghazali and G. P. Kusuma, "Indoor positioning system using regression-based fingerprint method," *Int. J. Adv. Comput. Sci. Appl. (IJACSA)*, vol. 10, no. 8, pp. 231–239, 2019.
- [45] D. Zhang and G. Lu, "Evaluation of similarity measurement for image retrieval," in *Proc. Neural Netw. and Signal Process.*, vol. 2, 2003, pp. 928–931.
- [46] P. Zhou, Y. Zou, X.-T. Yuan, J. Feng, C. Xiong, and S. Hoi, "Task similarity aware meta learning: Theory-inspired improvement on MAML," in *Proc. Uncertainty Artif. Intell. (UAI)*, 2021, pp. 23–33.
- [47] A. Gretton, K. M. Borgwardt, M. J. Rasch, B. Schölkopf, and A. Smola, "A kernel two-sample test," *J. Mach. Learn. Res.*, vol. 13, no. 1, pp. 723–773, 2012.
- [48] I. Steinwart, "On the influence of the kernel on the consistency of support vector machines," *J. Mach. Learn. Res.*, vol. 2, pp. 67–93, 2001.
- [49] K. Haneda, L. Tian, H. Asplund, J. Li, Y. Wang, D. Steer, C. Li, T. Balercia, S. Lee, Y. Kim *et al.*, "Indoor 5G 3GPP-like channel models for office and shopping mall environments," in *Proc. IEEE Int. Conf. Commun. Workshops*, 2016, pp. 694–699.
- [50] A. Bose and C. H. Foh, "A practical path loss model for indoor WiFi positioning enhancement," in *Proc. IEEE Int. Conf. Info. Commun. Signal Process.*, 2007, pp. 1–5.
- [51] 3GPP, "Study on channel model for frequencies from 0.5 to 100 GHz," *3rd Generation Partnership Project (3GPP), Tech. Rep. TR 38.901 V14.1.1 Release 14*, Aug. 2017. [Online]. Available: [Online].Available:<http://www.3gpp.org/DynaReport/38901.htm>